

Lift-the-Flap: Context Reasoning Using Object-Centered Graphs

Mengmi Zhang^{1,2,5}, Jiashi Feng¹, Karla Montejo³, Joseph Kwon⁴, Joo Hwee Lim², and Gabriel Kreiman⁵

Address correspondences to gabriel.kreiman@tch.harvard.edu

¹National University of Singapore, Singapore

²Institute for Infocomm Research, A*STAR, Singapore

³Mayo Clinic Graduate School of Biomedical Sciences, USA

⁴Yale University, USA

⁵Harvard Medical School, Boston Children’s Hospital, USA

Abstract

Children benefit from lift-the-flap books by taking on an active role in guessing what is behind the flap based on the context. In this paper, we introduce lift-the-flap games for computational models. The task is to reason about the scene context and infer what the target behind the flap is in a natural image. Context reasoning is critical in many computer vision applications, such as object recognition and semantic segmentation. To tackle this problem, we propose an object-centered graph representing the scene configuration of the image where each node corresponds to a group of objects belonging to the same category. To infer the target’s class label, we introduce an object-centered graph network model consisting of two sub-networks. The classification sub-network takes the complete graph as input and outputs a classification vector assigning the probability for each class. The reinforcement learning sub-network exploits the class label dependencies and learns the joint probability among objects in order to generate multiple reasonable answers for the missing target. To evaluate our model’s performance, we carry out human behavioral experiments for lift-the-flap games as a benchmark. Our model makes reasonable inferences compared to humans, and significantly outperforms all the null models. We also demonstrate the usefulness of our object-centered graph network model in context-aware object recognition and target priming in visual search.



Figure 1. Illustrative schematic of lift-the-flap games. The game requires players to capitalize on the scene context in a natural image to infer what is behind the flap (the blocked out target), out of a pre-defined set of object classes. The ground truth image at the bottom left (not shown in the actual experiments) reveals the target in the yellow bounding box.

in particular environments. Humans have the ability of exploiting contextual associations among objects in the environment. Contextual analysis, as the statistical summary of these relationships among objects, provides a complementary and effective source of information for perceptual inference tasks, such as object detection [37, 31, 14, 38, 24], scene classification [12, 39, 45], semantic segmentation [45], and visual question answering [35].

One example of how contextual information can be incorporated during recognition is lift-the-flap books, where children make guesses about what is behind the flap based on the context and check their answers by lifting the flap. We adopt the constructivist learning paradigm [17] as a computational model to solve lift-the-flap challenges. Through lift-the-flap images, the model can learn the

1. Introduction

The tiny object on the table is probably a spoon, not an elephant. In the real world, objects do not appear in isolation. Instead, they co-vary with other objects

statistical summary of scene context via reinforcement learning and supervised learning. Figure 1 illustrates the schematic of lift-the-flap games. Given a natural image with the target blocked by the flap, the goal of the game is to reason about the scene context and infer what the target is out of a pre-defined set of object classes.

David Marr’s object-centered approach to the study of vision has been highly influential [27]. In his approach, the positions of all objects in the scene are encoded with respect to a set of axes and an origin centered on the selected object. For example, from a computer monitor’s point of view, there is typically a mouse on its left and the mouse’s size is often smaller than the monitor itself. Physiological and neuropsychological results have supported the existence of such representations in humans and monkeys [6, 3]. Over viewer-centered representations, object-centered models are invariant to absolute object positions and area sizes at the pixel levels. Likewise, the combinatorial explosion due to multitude of imaginable views would lead to the rejection of viewer-centered representations. Inspired by this theory, we construct scene layouts in object-centered views and select the center of the blocked-out target as the origin. The positions and areas of other objects in the image can then be normalized with respect to the target. Mathematically, we formulate the scene layout as an object-centered graph. There are C nodes representing each object class and K node features including relative position, area, number of object instances in that class, and spreadness which describes the spatial distribution of these objects.

In contextual inference, there could be multiple reasonable answers. For example, in Figure 1, although the target is a bus (which can be obtained from the ground truth image), a car or a truck are also reasonable answers. While traditional multi-label classification approaches could train independent category classifiers and employ ranking or thresholding [42], they fail to exploit the predicted class label dependencies. Thus, in addition to classification, we introduce deep reinforcement learning on incremental graphs to encourage our model to explore all “reasonable” inferences by sequentially linking all nodes together and exploiting correlations among multiple predicted object classes. There are two advantages of making contextual inferences in a sequential manner. First, adding additional nodes on incremental graphs enables our model to pay attention to different object classes at each inference step. Second, inferring targets sequentially improves generalization because it explicitly exploits higher-order object relations and increases the number of training samples via rich permutations of node presentations. To avoid reward sparsity [20] during reinforcement learning, we provide intrinsic rewards as incentives at each inference step to ensure that our model learns the joint probability among object classes.

We design behavioral experiments to measure human performance in lift-the-flap games as a benchmark to evaluate our model. Our model performs contextual reasoning comparably well as humans and significantly outperforms other null models. Qualitative results suggest that our model makes multiple reasonable inferences even in cases where subjective solutions may not match the exact ground truth class. In the experiments, we demonstrate the usefulness of our object-centered graph network model in computer vision applications, such as context-aware object recognition task and target priming in visual search task.

In sum, our paper makes the following contributions:

- We introduce lift-the-flap games for computational models to learn context reasoning during the game.
- To model scene context, we propose object-centered graph representations. With respect to the blocked-out target in the image, all objects and their associations contribute to the model’s inference process irrespective of their absolute area sizes and positions at the pixel levels.
- To learn multi-label joint probability for the blocked-out target in context reasoning, we introduce a deep-Q-network on incremental graphs. During training, intrinsic rewards at each inference step motivate our model to pay attention to different nodes, exploit higher-order object correlations and improve generalization ability of target inference.
- We contribute behavioral experiments of lift-the-flap games for humans as a benchmark. Experimental results suggest that the accuracy of our model in context reasoning is comparable to human performance.

2. Related Work

We summarize context-aware computer vision applications and computational models of structural inference using graphs.

2.1. Role of Context in Computer Vision

Contextual reasoning about objects and relations is critical to machine vision. Here, we briefly summarize a few representative works in each application domain. A number of approaches employ contextual information in order to improve object detection [31, 14, 38, 24]. The types of contexts can be exploited in the form of global scene context [38], ground plane estimation [31], geometric context in the single image [14], relative location [8], 3D layout [22], and spatial support and geographic information [10]. In [12, 45, 21], researchers propose Conditional Random Field (CRF) models that reason jointly across multiple computer vision tasks in image labeling and

scene classification. Additionally, [30] studies the role of context in both object detection and semantic segmentation tasks, demonstrating improved performance in both tasks compared to raw image features. Recently, several neural network architectures incorporating contextual information have been successfully applied in object priming [37], place and object recognition [43, 39], object detection [24] and visual question answering [35].

In contrast to all these works designing specific contextual reasoning frameworks for different computer vision applications, we propose a generic computational model for contextual reasoning which can act as a separate functional module and combine with state-of-the-art computer vision models for various applications.

2.2. Structural Inference with Graphs

There are several interesting approaches to address the problem of combining graphical models with deep neural networks for structural inference, primarily in structured prediction tasks [26, 5, 4, 35, 15, 2, 44]. [15] designs a structured model to improve classification performance by leveraging relations among scenes, objects and their attributes. A structured inference model is also used in [5, 7] for analyzing relations in group activity recognition. Several works, like Structural-RNN [16] and Interaction Net [2], combine the power of spatiotemporal graphs and sequence learning, and evaluate the model from motion prediction to object interactions. [4] proposes DeepLab which inputs the response at the final layer of a deep neural network to CRF model for semantic image segmentation. Subsequently, [32, 46] transforms the CRF model into a Recurrent Neural Network in an end-to-end fashion.

Breaking away from previous work where graphs are constructed in a view-dependent manner, we focus on object-centered graphs which are invariant to absolute object positions and area sizes at pixel level. In addition to tackling context reasoning problems using supervised learning like previous works, we propose a complementary sub-network via reinforcement learning which learns to capture the joint-probability among object classes while predicting multiple labels for the blocked-out target.

3. Our Model

We first provide an overview of our proposed model, Object-Centered Graph Network (OCGN) (Figure 2), followed by a detailed description of its architecture.

3.1. Architecture Overview

Given a natural image I with a target region blocked out, we retrieve the ground truth bounding boxes and class labels of all visible objects in the image. We formulate the scene layout as object-centered graphs and set the blocked-out target as the origin. The positions and areas of all objects

can then be normalized with respect to the target region. In the graph, each node represents one object class containing features of all object instances belonging to that class.

Our proposed **OCGN** model consists of two sub-networks: graph classification network (**GCN**) and graph deep-Q-network (**GDQN**). In **GCN**, the network takes the object-centered graph as input and outputs a classification vector which assigns the probability that the target region contains an object of each class. As we also want our model to predict multiple reasonable answers that are close to the ground truth, we motivate the model to learn class label dependencies by deciphering class-to-class relations on incremental graphs where one more node is added to the graph at each inference step t . Contextual reasoning in a sequential manner enables **GDQN** to focus on different object classes at every inference step t and improve its generalization ability by explicitly exploiting higher-order object class relations on rich permutations of node presentation sequences. **GDQN** outputs the predicted Q-value for each action where each action corresponds to a class label. To avoid reward sparsity [20], **GDQN** accumulates intrinsic rewards on incremental graphs until the graph covers all objects in the image. We define the rewards as a function of degree measuring how reasonable the predicted class is compared with the ground truth. At the last inference step T , we fuse the predicted Q values from **GDQN** with the classification vector from **GCN** via element-wise multiplication. The class with the maximum belief is the inferred target’s class label.

3.2. Object-Centered Graph

There are C object classes in total. In the image I , we define the object-centered graph $G = \langle D, E, R \rangle$ as an attributed, directed graph with its nodes D always pointing from the central node d_c (the blocked-out target region) to other nodes d_j (groups of object instances belonging to class C_j). In lift-the-flap games, we deal with object-centered static graphs and there are no motion dynamics. Thus, we can greatly simplify the graph representation G as a matrix of size $C \times K$ with all its K features of neighboring nodes d_j normalized with respect to d_c .

We assume that there are N known objects on the image I where $o_i \in \{o_1, o_2, \dots, o_N\}$ and the blocked-out target region o_c . Each object o_i has the following attributes: position (px_{o_i}, py_{o_i}) normalized with respect to the width and height of the image I , its area size A_{o_i} normalized with respect to the total size of the image I and its class label c_{o_i} .

We group all objects o_i having the same class label and extract their features for node d_j . A tuple with $K = 6$ entries describes the node features: relative position (p_{j1}, p_{j2}) , area size p_{j3} , spatial distribution (p_{j4}, p_{j5}) , and number of object instances p_{j6} belonging to class C_j :

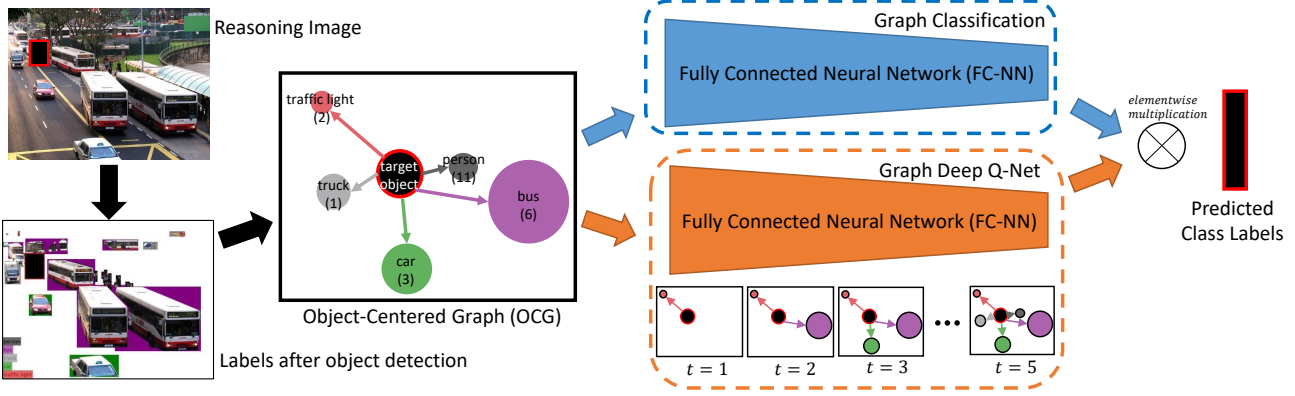


Figure 2. Architecture of our proposed Object Centered Graph Network (OCGN) model. The model consists of two independent sub-networks, **Graph Classification Network (GCN)** (blue shade) and **Graph Deep Q-Network (GDQN)** (orange shade). Given the natural image with the target blocked out, we retrieve the ground truth bounding boxes and class labels of all objects on the image. Based on the scene configuration, we construct an object-centered graph with respect to the blocked target (see text). The number in brackets denotes the number of object instances on the image belonging to that class. The graph is input to **GDQN** in a sequential manner. At each inference step t , one more node is added to the graph. **GDQN** learns to accumulate rewards across inference steps until the graph is complete. **GCN** takes the complete graph as inputs and outputs the predicted classification vector assigning probability for each class label. At the last inference step, the learnt Q values for all class labels from **GDQN** are normalized within $[0, 1]$ and fused with the classification vector from **GCN** via element-wise multiplication. The class with the maximum belief is the predicted class label for the missing target.

$$p_{j1} = \frac{1}{p_{j6}} \sum_{c_{oi} \in C_j} (px_{oi} - px_{oc}), \quad (1)$$

$$p_{j2} = \frac{1}{p_{j6}} \sum_{c_{oi} \in C_j} (py_{oi} - py_{oc}), \quad (2)$$

$$p_{j3} = \frac{1}{(p_{j6} \times A_{oc})} \sum_{c_{oi} \in C_j} A_{oi}, \quad (3)$$

$$p_{j4} = \max_{c_{oi} \in C_j} \{px_{oi} - px_{oc}\} - \min_{c_{oi} \in C_j} \{px_{oi} - px_{oc}\}, \quad (4)$$

$$p_{j5} = \max_{c_{oi} \in C_j} \{py_{oi} - py_{oc}\} - \min_{c_{oi} \in C_j} \{py_{oi} - py_{oc}\}, \quad (5)$$

$$p_{j6} = |\{oi | c_{oi} \in C_j\}| \quad (6)$$

where $|\cdot|$ denotes the cardinality of a set. In the graph, the node d_j is valid if there is at least one object belonging to that class; otherwise, we treat d_j as a dummy node with all its entries set as zero. This is due to the constraint that our feed-forward network can only take fixed-size graph input. Thus, the object-centered graph G can be represented as the following matrix of size $C \times 6$:

$$G = \begin{bmatrix} p_{11} & \cdots & p_{16} \\ \vdots & \ddots & \vdots \\ p_{C1} & \cdots & p_{C6} \end{bmatrix}_{C \times 6} \quad (7)$$

where

$$p_{ji} = 0, i = \{1, 2, 3, 4, 5\}, \text{ if } p_{j6} = 0$$

In order to study the individual role of these node features, we conduct a node feature ablation study. See

Supplementary Material for performance on the ablated object-centered graphs.

3.3. Graph Classification Network

We flatten the complete graph G as a vector of size $C \times K$ as input to the graph classification network which is a feed-forward fully-connected neural network. It outputs the classification vector of size C with each value corresponding to the predicted probability of each class. Similar as typical classification problems in machine learning, we train **GCN** using cross-entropy loss in a supervised manner:

$$L_{classi} = - \sum_{c=1}^C y_c \ln(p_c) \quad (8)$$

where y_c is a binary indicator representing whether class c is the ground truth and p_c is the predicted probability of class c .

3.4. Graph Deep-Q Network

In lift-the-flap games, although there is only one correct answer to the blocked-out target in the image I , there could be multiple subjective answers which are also reasonable. The classification loss in Eqn. 8 penalizes all the wrong predictions equally. In order to encourage our model to actively explore all subjective answers and learn the object class label dependencies, we propose a deep-Q-network on graphs. Complementary to **GCN**, it estimates the multi-label joint distribution by exploiting class-to-class correlations in a sequential manner.

Deep reinforcement learning has achieved notable successes in various tasks, such as robotic control [1] and the game of Go [33]. In particular, deep-Q-network [29] is a scalable model-free approach which maps current states to an action space by predicting the Q-values for each action. During training, the agent interacts with the environment via a set of actions and learns the best policy which maximizes cumulative rewards.

In context reasoning, we present **GDQN** with the incremental graph G_t as the states of the environment. At each inference step t , one more valid node is added to the existing graph until there is no more valid node left. This facilitates **GDQN** to focus on different object classes in the image during target inference and improves its generalization ability in contextual reasoning. During training, the sequence of valid node presentation is randomized to prevent overfitting and encourage exploitation of higher order class-to-class correlations.

GDQN is a feed-forward fully-connected neural network with parameters θ . It outputs the predicted Q values over all actions. We define the action space a_i to be C classes where $i = \{1, 2, 3, \dots, C\}$. In other words, **GDQN** has to make inferences about what the blocked-out target is given the incremental graph G_t at each inference step t .

To measure how reasonable the inferred target class c_t is compared with the ground truth class c_g at inference step t , we define an intrinsic reward r_t as a function $f_r(\cdot)$:

$$r_t = f_r(c_t, c_g) = 1 - \frac{f_w(c_t, c_g)}{\max_{j \in C} \{f_w(c_j, c_g)\}} \quad (9)$$

where $f_w(\cdot)$ is a function returning the number of traversing words between the target class label and the ground truth label based on WordNet [28]. WordNet is a lexical dataset in a hierarchical tree structure for English language.

To avoid the two divergence problems in deep reinforcement learning: high correlations between adjacent experiences, and easy-forgetting of past learning experiences, we adopt the same strategy of memory replay as [29]. We randomize the sequence of episodes in the memory and update θ to θ^- with frequency f_M . The loss function for **GDQN** is defined as below:

$$L_Q = (r_t + \gamma \max_{c_t} Q(G_{t-1}, c_t, \theta^-) - Q(G_t, c_t, \theta))^2 \quad (10)$$

where γ is the discount factor.

3.5. Implementation Details

Both **GCN** and **GDQN** have the same network architecture but the weights are not shared between each other. Both networks consist of 5 fully-connected (fc) blocks (fc + relu activation): fc1 (4096), relu, fc2 (2048), relu, fc3 (1024), relu, fc4 (1024), relu, and fc5 (C).

We train both sub-networks, **GCN** and **GDQN**, separately. In **GCN** training, we take inputs of batch size 256 and train the network using Adam optimizer [18] with learning rate 0.0005. In **GDQN** training, we take inputs of batch size 512, and train the network using RMSprop optimizer [36] with learning rate 0.00025. We set the replay memory size as 2,500, the network parameter θ update frequency $f_M = 1,000$ and the discount factor $\gamma = 0.95$. We will make our source code, pre-trained models, and human behavioral experiment data publicly available upon publication.

4. Experiments

4.1. Datasets

Dataset for Behavioral Experiments from MSCOCO

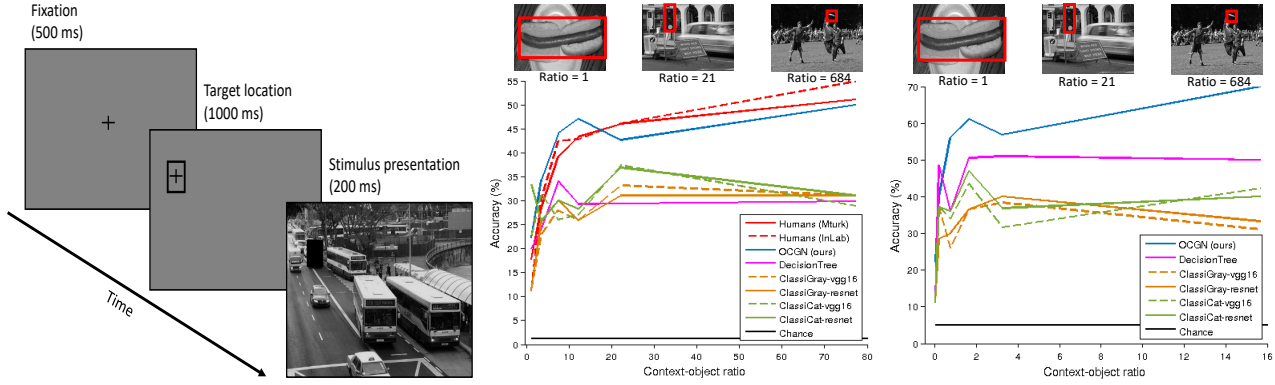
We analyze images from the MSCOCO Dataset [23] spanning 80 object categories including cars, dogs, clocks, etc. This dataset has been widely used for object recognition and detection [23]. We use all images from the MSCOCO training set for training and validation. On every training image, each object can be blocked out as the missing target, which results in roughly 570,000 object-centered graphs. In the MSCOCO validation set, we randomly select 573 natural images for human behavioral experiments. To avoid memory effects, we choose ONLY one missing target on every test image; otherwise, the same human subject may be presented with the same image twice but with a different blocked-out target each time. Meanwhile, we make sure there is no bias in object class distributions. Within each class, the number of test images with different ratios of contextual information versus blocked-out target size is uniform.

We design the human behavior experiments on the selected 573 test images from MSCOCO Dataset. See schematic in Figure 3a and Supplementary Material for more implementation details.

PASCAL Dataset To scale up our test set, we also include all the images from the training set in PASCAL Dataset [11] except for those images containing one single object. The PASCAL Dataset spans over 20 object categories and contains rich annotations for object recognition and segmentation tasks. As these 20 object categories are a subset of the 80 ones from the MSCOCO Dataset, we directly test our pre-trained model from MSCOCO Dataset on these images without any fine-tuning. During the target inference, we treat the remaining 60 classes as invalid classes and exclude them for evaluation.

4.2. Evaluation Metrics

We evaluate our **OCGN** model on MSCOCO and PASCAL Datasets using the typical classification accuracy measure. As we are interested in studying the role



(a) Schematics of Behavioral Experiment

(b) MSCOCO Dataset

(c) PASCAL Dataset

Figure 3. Schematic illustration of human behavioral experiments and evaluation of context reasoning accuracy as a function of context-object ratio. (a) Human behavioral experiments. After fixation, the blocked-out target is described in the form of a bounding box with a fixation cross in the center of the box, presented for 1,000 ms. After that, the grayscale natural image appears for 200 ms. Subjects are instructed to use a noun to describe what the blocked-out target is either verbally in the experiments conducted in the lab or typed in a text box in the experiments conducted online using AmazonTurk [41]. (b) Human and model performance on MSCOCO Dataset. (c) Model performance on PASCAL Dataset. Context reasoning accuracy is a function of context-object ratio. (Sec. 4.2). Three example images with different context-object ratios are presented on the top. Both the red solid and dash lines correspond to human performance. The other lines denote different models: OCGN (blue, our proposed Object-Centered Graph Network), DecisionTree (cyan, decision trees on graphs), ClassiGray (orange, classification on natural images with the target blocked out using VGG16 [34] in dash line and ResNet [13] in solid line), ClassiCat (green, classification on segmented images using VGG16 in dash line and ResNet in solid line), Chance (black).

of context in the target inference process, we report the contextual reasoning accuracy, *i.e.* top-1 classification accuracy, as a function of context-object ratio. Given an image I , the context-object ratio is defined as the total area of the image EXCLUDING the missing target size divided by the missing target size. For example, the context-object ratio of 1 implies equal context and target sizes in the image.

4.3. Comparative Null Models

We compare our model with several alternative null models and report their performance in Figure 3. In all cases, the alternative models predict the class probability for the missing target.

Chance. We consider a model where the predicted class is chosen at random. As there are 80 classes in MSCOCO Dataset and 20 in PASCAL Dataset, the accuracies at chance are 1/80 and 1/20 respectively.

DecisionTree. A decision tree [9] is a tree-structured model of decisions and consequences. It has been commonly used in the machine learning literature. In each image, the tree takes the vectorized object-centered graph G as input and outputs the predicted class label.

ClassiGray. A naive way of inferring the class label is to perform classification directly on the natural image with the missing target. We fine-tune state-of-the-art 2D-Convolution Neural Networks for object recognition, including VGG16 [34] (ClassiGray-vgg16) and ResNet [13] (ClassiGray-resnet), using cross-entropy loss on the natural images where the targets are blocked out. To be

consistent with human behavioral experiments, all natural images are in grayscale.

ClassiCat. The object-centered graph is constructed based on the ground truth bounding box labels of the image. For fair comparison, we segment the image based on ground truth labels and assign a pre-defined grayscale value to each class, background, and the blocked-out target region respectively. We fine-tune state-of-the-art object recognition networks including VGG16 [34] (ClassiCat-vgg16) and ResNet [13] (ClassiCat-resnet) on these segmented images using cross-entropy loss and test its classification performance on the test set.

4.4. Results on Context Reasoning

Figure 3 shows human and model performance in context reasoning on MSCOCO Dataset (Figure 3b) and PASCAL Dataset (Figure 3c).

It is observed that the performance of both humans and all models improves monotonically with increasing context-object ratio. This reveals the important role of context in structural inference.

In Figure 3b, in-lab subjects (red, dash line) are able to infer the missing target with 31% accuracy when the context-object ratio is 3.4 on average and 55% at the context-object ratio of 77. The turkers' performance (red, solid line) is consistent with in-lab subjects' performance in terms of target inference accuracy of 29% and 51% at the context-ratio of 3.4 and 77 respectively. The contextual reasoning task is quite hard, as indicated by the maximum

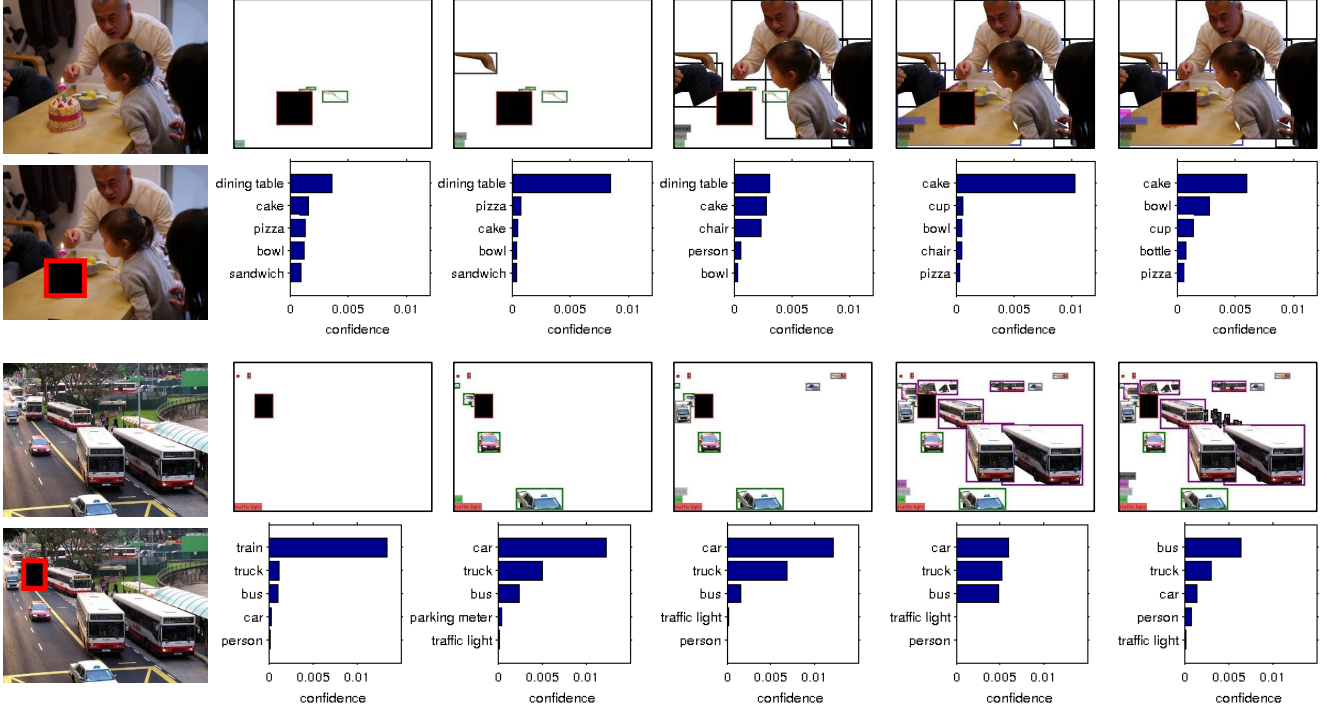


Figure 4. Example results of context reasoning. Every two rows corresponds to a separate example. In the first column of each example, the images from top to bottom are: the ground truth with the target revealed, and the stimuli with the target blocked out (red bounding box). In the second column and onwards, the first row shows the visualization of incremental graphs G_t at image level. The second row shows their corresponding histograms representing the confidence of top-5 predicted object classes for the target object by our proposed Object-Centered Graph Network model on G_t . The x-axis denotes the confidence. The y-axis shows the top-5 predicted object class labels.

performance of 51% for humans. In other words, subjects cannot correctly infer what the object is in half of the trials. We provide analysis on the patterns of mistakes that humans make in Supplementary Material. It is observed that though the inferred target class labels do not exactly match with the ground truth, they are still “reasonable” in terms of word-to-word distances. For example, the ground truth target is a bus in Figure 1 but a car is also a reasonable guess compared to guessing an elephant.

Our **OCGN** model (blue) performs competitively well with humans and surpasses all the alternative null models. On MSCOCO Dataset, it achieves the target inference accuracy as high as 34% at the context-object ratio of 3.4 and 50% at the ratio of 77. We should be cautious that the comparable performances between humans and our model cannot be over-interpreted, as humans have the freedom to describe the missing target using any nouns, while our model has to infer the target’s category out of a pre-defined set of object classes.

Across both datasets, all the alternative null models outperform Chance (black), which implies that they all capture some essential features for context reasoning. ClassiGray (brown) is the most direct approach for tackling context reasoning, but its performance is the lowest among

all null models. It is possible that although 2D-Convolution Neural Network takes spatial information into account at the pixel levels, it fails to capture the scene configuration in a holistic viewpoint with higher level class correlation structure. With the ground truth segmentation information given, ClassiCat (green) is still inferior to ours because our model could analyze the scene configurations in a view-independent fashion. Lastly, classification on graphs using decision tree (cyan) does not perform as well as our model. This confirms that deep neural networks can automatically learn the graph patterns in the high-dimensional space for contextual reasoning.

In Figure 4, we provide two qualitative examples of the top-5 inferred target’s class labels on each incremental graph G_t . These visualization examples help us gain insights of the contextual inference process of our **OCGN** model. For example, in the first visualization result (first two rows), given only two forks (Column 2, $t = 1$), our model infers there is probably a dining table. It is also observed that the other top three inferred object classes (cake, pizza, sandwich) are from food super-category. All these predictions are reasonable guesses which suggest that our model captures the multi-label joint probability from **GDQN** even with little contextual information. As more

accuracy (%)	top-1	top-3	top-5
VGG16 [34]	64.9	83.1	88.7
VGG16 + ClassiGray-VGG16	71.2	87.3	92.1
VGG16 + ClassiCat-VGG16	73.6	90.8	92.7
VGG16 + OCGN (ours)	78.9	90.8	94.7
ResNet [13]	64.0	82.0	89.9
ResNet + ClassiGray-ResNet	70.3	85.5	90.2
ResNet + ClassiCat-ResNet	73.8	87.3	92.8
ResNet + OCGN (ours)	76.4	88.8	92.8

Table 1. Model object recognition accuracy on 573 randomly selected targets from grayscale natural images in MSCOCO. See Supplementary Material for detailed description of each computational model. The best performance is highlighted in bold.

valid nodes are added to the graph G_t , our model updates its belief from a relatively uniform posterior distribution (Column 2, $t = 1$) to a multimodal distribution (Column 3, $t = 2$). When there is a dining table covering most part of the image (Column 5, $t = 4$), the model updates its belief to the correctly inferred target class (cake). With the addition of the bowl on the table, it changes the overall distribution though the mode of the distribution remains. What is also interesting is that our model seems to learn the consistency effect of context: given a bowl on the table, its nearby object is also probably a bowl or at least similar types of containers (Column 6, $t = 5$).

We use t-SNE visualization method [25] to map latent graph representations into a 2D space and examine the clusters based on the class labels of the missing targets given different amount of contextual information. See Supplementary Material for t-SNE visualization results. Comparing the two results, we observe more distinctive clusters when there are more objects in the image. This confirms GCN capitalizes on contextual information to make inferences. More contextual information ascribes to more distinct clusters that are representative of individual object classes.

4.5. Context Aware Object Recognition

We demonstrate the usefulness of our OCGN model in object recognition on MSCOCO. Table 1 reports the accuracies for the minimal context and full context conditions. From top to bottom, object recognition on the minimal context has the worst performance. *e.g.* VGG16 [34], a 2D-Convolution Neural Network using minimal context, has the top-1 accuracy of 64.9% on MSCOCO while full-context models, such as our model, achieve top-1 accuracy as high as 78.9%.

Compared to object recognition accuracy of about 80% using ResNet [13] on ImageNet [19], the accuracy in minimal context is relatively lower on MSCOCO. One possible reason is that these objects are usually cropped from complex images (high context-object ratio) and are of low resolution. As objects do not often occur in isolation

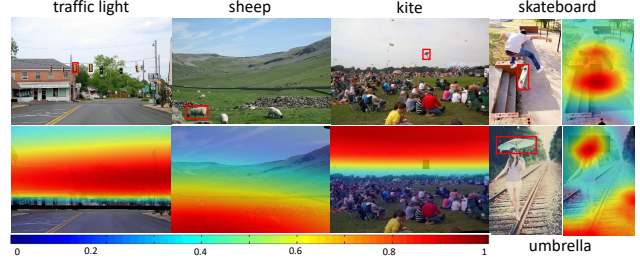


Figure 5. Example results of generated target-driven priming maps in visual search by our Object-Centered Graph Network model. Each example includes the search image with the ground truth target location in red bounding box and the target-driven priming maps overlaid indicating where the target is most likely to be in the search images. The target class labels are given on the top.

in reality, this validates the importance of context in object recognition.

Table 1 shows our OCGN model achieves an increased performance of around 7% and 4% in top-1 accuracy on MSCOCO compared with the context-aware ClassiGray and ClassiCat respectively. It validates that the high-level structure of class correlations is helpful for object recognition. Over view-dependent graphs, object-centered graphs are invariant to absolute object positions and area sizes in pixels and their graph representations of scene configurations are more useful for object recognition.

4.6. Context Aware Object Priming

Object priming refers to a guidance process of the subsequent stimuli given the prior exposure to the current stimulus. Torralba *et al.* [40] prove that object priming enables efficient attention allocation during a visual search task in a natural environment. For example, if the search task is to look for cars, humans usually skip over large areas in the sky and focus their attention on the streets.

In Figure 5, we provide visualization examples of the generated target-driven priming maps which are 2D probabilistic maps indicating where the target is most likely to be in the search images by our OCGN model. See Supplementary Material for implementation details. The red color denotes more probable target locations. It is visually intuitive that our OCGN model generates reasonable target priming maps. For example, the traffic light is most likely to be above the streets; the sheep are on the grass and the kites are in the sky. It is also interesting that our model also captures multi-modal prior distributions for certain types of targets. For example, skateboards could be either in front of or below the person; and the umbrella could be in front of or above the person.

5. Conclusion

Inspired by context-driven learning of scene configuration in children playing lift-the-flap games, we introduce a target inference task for computational models. To represent relations among objects, we propose object-centered graphs. To correctly infer the target's class labels, we train our model using supervised classification loss on complete graphs and deep reinforcement learning on incremental graphs. Experimental results suggest that our model has human-like contextual reasoning behaviors and its contextual reasoning ability is useful in object recognition and object priming tasks.

There are some aspects that our current computational model can improve on. First, we hand-craft node features from raw pixels. Second, we only consider relations among objects and the global scene information is discarded.

References

- [1] S. Amarjyoti. Deep reinforcement learning for robotic manipulation-the state of the art. *arXiv preprint arXiv:1701.08878*, 2017. 5
- [2] P. Battaglia, R. Pascanu, M. Lai, D. J. Rezende, et al. Interaction networks for learning about objects, relations and physics. In *Advances in neural information processing systems*, pages 4502–4510, 2016. 3
- [3] I. Biederman. Human image understanding: Recent research and a theory. *Computer vision, graphics, and image processing*, 32(1):29–73, 1985. 2
- [4] L.-C. Chen, G. Papandreou, I. Kokkinos, K. Murphy, and A. L. Yuille. Deeplab: Semantic image segmentation with deep convolutional nets, atrous convolution, and fully connected crfs. *IEEE transactions on pattern analysis and machine intelligence*, 40(4):834–848, 2018. 3
- [5] W. Choi and S. Savarese. A unified framework for multi-target tracking and collective activity recognition. In *European Conference on Computer Vision*, pages 215–230. Springer, 2012. 3
- [6] S. Deneve and A. Pouget. Basis functions for object-centered representations. *Neuron*, 37(2):347–359, 2003. 2
- [7] Z. Deng, A. Vahdat, H. Hu, and G. Mori. Structure inference machines: Recurrent neural networks for analyzing relations in group activity recognition. In *Proceedings of the IEEE Conference on Computer Vision and Pattern Recognition*, pages 4772–4781, 2016. 3
- [8] C. Desai, D. Ramanan, and C. C. Fowlkes. Discriminative models for multi-class object layout. *International journal of computer vision*, 95(1):1–12, 2011. 2
- [9] T. G. Dietterich. Ensemble methods in machine learning. In *International workshop on multiple classifier systems*, pages 1–15. Springer, 2000. 6
- [10] S. K. Divvala, D. Hoiem, J. H. Hays, A. A. Efros, and M. Hebert. An empirical study of context in object detection. In *Computer Vision and Pattern Recognition, 2009. CVPR 2009. IEEE Conference on*, pages 1271–1278. IEEE, 2009. 2
- [11] M. Everingham, L. Van Gool, C. K. Williams, J. Winn, and A. Zisserman. The pascal visual object classes (voc) challenge. *International journal of computer vision*, 88(2):303–338, 2010. 5
- [12] J. M. Gonfaus, X. Boix, J. Van de Weijer, A. D. Bagdanov, J. Serrat, and J. Gonzalez. Harmony potentials for joint classification and segmentation. In *Computer Vision and Pattern Recognition (CVPR), 2010 IEEE Conference on*, pages 3280–3287. IEEE, 2010. 1, 2
- [13] K. He, X. Zhang, S. Ren, and J. Sun. Deep residual learning for image recognition. In *Proceedings of the IEEE conference on computer vision and pattern recognition*, pages 770–778, 2016. 6, 8
- [14] D. Hoiem, A. A. Efros, and M. Hebert. Geometric context from a single image. In *Computer Vision, 2005. ICCV 2005. Tenth IEEE International Conference on*, volume 1, pages 654–661. IEEE, 2005. 1, 2
- [15] H. Hu, G.-T. Zhou, Z. Deng, Z. Liao, and G. Mori. Learning structured inference neural networks with label relations. In *Proceedings of the IEEE Conference on Computer Vision and Pattern Recognition*, pages 2960–2968, 2016. 3
- [16] A. Jain, A. R. Zamir, S. Savarese, and A. Saxena. Structural-rnn: Deep learning on spatio-temporal graphs. In *Proceedings of the IEEE Conference on Computer Vision and Pattern Recognition*, pages 5308–5317, 2016. 3
- [17] M. S. Jong, J. Shang, and F.-I. Lee. Constructivist learning through computer gaming. In *Technologies shaping instruction and distance education: new studies and utilizations*, pages 207–222. IGI Global, 2010. 1
- [18] D. P. Kingma and J. Ba. Adam: A method for stochastic optimization. *arXiv preprint arXiv:1412.6980*, 2014. 5
- [19] A. Krizhevsky, I. Sutskever, and G. E. Hinton. Imagenet classification with deep convolutional neural networks. In *Advances in neural information processing systems*, pages 1097–1105, 2012. 8
- [20] T. D. Kulkarni, K. Narasimhan, A. Saeedi, and J. Tenenbaum. Hierarchical deep reinforcement learning: Integrating temporal abstraction and intrinsic motivation. In *Advances in neural information processing systems*, pages 3675–3683, 2016. 2, 3
- [21] L. Ladicky, C. Russell, P. Kohli, and P. H. Torr. Graph cut based inference with co-occurrence statistics. In *European Conference on Computer Vision*, pages 239–253. Springer, 2010. 2
- [22] D. Lin, S. Fidler, and R. Urtasun. Holistic scene understanding for 3d object detection with rgbd cameras. In *Proceedings of the IEEE International Conference on Computer Vision*, pages 1417–1424, 2013. 2
- [23] T.-Y. Lin, M. Maire, S. Belongie, J. Hays, P. Perona, D. Ramanan, P. Dollár, and C. L. Zitnick. Microsoft coco: Common objects in context. In *European conference on computer vision*, pages 740–755. Springer, 2014. 5
- [24] Y. Liu, R. Wang, S. Shan, and X. Chen. Structure inference net: Object detection using scene-level context and instance-level relationships. In *Proceedings of the IEEE Conference on Computer Vision and Pattern Recognition*, pages 6985–6994, 2018. 1, 2, 3

- [25] L. v. d. Maaten and G. Hinton. Visualizing data using t-sne. *Journal of machine learning research*, 9(Nov):2579–2605, 2008. 8
- [26] K. Marino, R. Salakhutdinov, and A. Gupta. The more you know: Using knowledge graphs for image classification. *arXiv preprint arXiv:1612.04844*, 2016. 3
- [27] D. Marr. *Vision: A computational investigation into*. WH Freeman, 1982. 2
- [28] G. A. Miller. Wordnet: a lexical database for english. *Communications of the ACM*, 38(11):39–41, 1995. 5
- [29] V. Mnih, K. Kavukcuoglu, D. Silver, A. A. Rusu, J. Veness, M. G. Bellemare, A. Graves, M. Riedmiller, A. K. Fidjeland, G. Ostrovski, et al. Human-level control through deep reinforcement learning. *Nature*, 518(7540):529, 2015. 5
- [30] R. Mottaghi, X. Chen, X. Liu, N.-G. Cho, S.-W. Lee, S. Fidler, R. Urtasun, and A. Yuille. The role of context for object detection and semantic segmentation in the wild. In *Proceedings of the IEEE Conference on Computer Vision and Pattern Recognition*, pages 891–898, 2014. 3
- [31] D. Park, D. Ramanan, and C. Fowlkes. Multiresolution models for object detection. In *European conference on computer vision*, pages 241–254. Springer, 2010. 1, 2
- [32] A. G. Schwing and R. Urtasun. Fully connected deep structured networks. *arXiv preprint arXiv:1503.02351*, 2015. 3
- [33] D. Silver, A. Huang, C. J. Maddison, A. Guez, L. Sifre, G. Van Den Driessche, J. Schrittwieser, I. Antonoglou, V. Panneershelvam, M. Lanctot, et al. Mastering the game of go with deep neural networks and tree search. *nature*, 529(7587):484, 2016. 5
- [34] K. Simonyan and A. Zisserman. Very deep convolutional networks for large-scale image recognition. *arXiv preprint arXiv:1409.1556*, 2014. 6, 8
- [35] D. Teney, L. Liu, and A. van den Hengel. Graph-structured representations for visual question answering. *arXiv preprint*, 2017. 1, 3
- [36] T. Tieleman and G. Hinton. Divide the gradient by a running average of its recent magnitude. coursera: Neural networks for machine learning. Technical report, Technical Report.(accessed on 21 April 2017). 5
- [37] A. Torralba. Contextual priming for object detection. *International journal of computer vision*, 53(2):169–191, 2003. 1, 3
- [38] A. Torralba, K. Murphy, and W. Freeman. Using the forest to see the trees: Ob-ject recognition in contex. *Comm. of the ACM*, 2010. 1, 2
- [39] A. Torralba, K. P. Murphy, and W. T. Freeman. Contextual models for object detection using boosted random fields. In *Advances in neural information processing systems*, pages 1401–1408, 2005. 1, 3
- [40] A. Torralba, A. Oliva, M. S. Castelhano, and J. M. Henderson. Contextual guidance of eye movements and attention in real-world scenes: the role of global features in object search. *Psychological review*, 113(4):766, 2006. 8
- [41] A. M. Turk. Amazon mechanical turk. *Retrieved August*, 17:2012, 2012. 6
- [42] J. Wang, Y. Yang, J. Mao, Z. Huang, C. Huang, and W. Xu. Cnn-rnn: A unified framework for multi-label image classification. In *Proceedings of the IEEE conference on computer vision and pattern recognition*, pages 2285–2294, 2016. 2
- [43] K. Wu, E. Wu, and G. Kreiman. Learning scene gist with convolutional neural networks to improve object recognition. In *Information Sciences and Systems (CISS), 2018 52nd Annual Conference on*, pages 1–6. IEEE, 2018. 3
- [44] D. Xu, Y. Zhu, C. B. Choy, and L. Fei-Fei. Scene graph generation by iterative message passing. In *Proceedings of the IEEE Conference on Computer Vision and Pattern Recognition*, volume 2, 2017. 3
- [45] J. Yao, S. Fidler, and R. Urtasun. Describing the scene as a whole: Joint object detection, scene classification and semantic segmentation. In *Computer Vision and Pattern Recognition (CVPR), 2012 IEEE Conference on*, pages 702–709. IEEE, 2012. 1, 2
- [46] S. Zheng, S. Jayasumana, B. Romera-Paredes, V. Vineet, Z. Su, D. Du, C. Huang, and P. H. Torr. Conditional random fields as recurrent neural networks. In *Proceedings of the IEEE international conference on computer vision*, pages 1529–1537, 2015. 3